TiO$_2$ Band Restructuring by B and P Dopants

Lei Li[1], Fanling Meng[1], Xiaoying Hu[2], Liang Qiao[2], Chang Q Sun[3], Hongwei Tian[1]*, Weitao Zheng[1]*

1 Department of Materials Science and Key Laboratory of Automobile Materials of MOE and State Key Laboratory of Superhard Materials, Jilin University, Changchun, China, **2** College of Science, Changchun University, Changchun, China, **3** School of Electrical and Electronic Engineering, Nanyang Technological University, Singapore, Singapore

* wtzheng@jlu.edu.cn (WTZ); tianhw@jlu.edu.cn (HWT)

Abstract

An examination of the effect of B- and P-doping and codoping on the electronic structure of anatase TiO$_2$ by performing density functional theory calculations revealed the following: (i) B- or P-doping effects are similar to atomic undercoordination effects on local bond relaxation and core electron entrapment; (ii) the locally entrapped charge adds impurity levels within the band gap that could enhance the utilization of TiO$_2$ to absorb visible light and prolong the carrier lifetime; (iii) the core electron entrapment polarizes nonbonding electrons in the upper edges of the valence and conduction bands, which reduces not only the work function but also the band gap; and (iv) work function reduction enhances the reactivity of the carriers and band gap reduction promotes visible-light absorption. These observations may shed light on effective catalyst design and synthesis.

Introduction

Because of its high chemical stability, high photocatalytic activity, and non-toxicity, titanium dioxide has been considered one of the more promising photocatalysts for photoelectrochemical water splitting, dye-sensitized solar absorption, degradation of pollutants, and fuel conversion. However, the undesirably fast rate of carrier recombination and the large band gap (3.0 eV for the rutile phase, 3.2 eV for the anatase phase) for photon absorption limits its practical applications.

In order to improve the catalytic efficiency of TiO$_2$, one needs to consider the following three parameters: (i) how to narrow the band gap from 3.2 eV to match the energy of high-intensity visible light, (ii) how to increase the electroaffinity of the specimen to prolong the lifetime of the carriers, and (iii) how to decrease the work function to improve the reactivity of the carriers. The electroaffinity is the separation between the bottom of the conduction band and the vacuum level, which describes the ability of the specimen to hold electrons captured during reaction or to entrap the conduction electrons that localize and polarize nonbonding electrons [1]. In the process of photocatalytic, when the reduction and oxidation do not proceed simultaneously, there is an electron accumulation in the conduction band, thereby causing a fast recombination of e-h pairs. Therefore, improve the utilization rate of sunlight by modulating band gap and enhance electrons lifetime by reducing the work function and increasing the

electroaffinity via locally pinning the polarized electrons are essential to promote photocatalytic reaction.

We have recently shown [2] that atomic undercoordination, such as a defect or a terrace edge formation, and nanocrystallization could improve the three quantities in the previous paragraph due to the bond order-length-strength correlation and nonbonding electron polarization (BOLS-NEP) mechanism [1]. The BOLS-NEP notation indicates that a loss of bond order shortens and stiffens the bonds between undercoordinated atoms [2, 3]. This event leads to the local densification and quantum entrapment of the bonding electrons to deepen the bottom edge of the energy bands, which polarizes the nonbonding electrons to shift up the upper edge of the bands. The conduction band edge depression increases the electroaffinity, which prolongs the carrier life. The polarization decreases the work function. On the other hand, atomic heterocoordination, such as what occurs with foreign-ion doping or codoping [4–10], surface sensitization by metal complexes or organic dyes [11, 12], noble metal loading [13, 14], and semiconductor coupling [15, 16], also exhibit the BOLS-NEP effect but to different extents.

Opinions about the B- and P-doping effects on the photoactivity of TiO$_2$ remain controversial though studies have been frequent. Chen et al. [17] observed that B-doping widens the band gap and attributed this observation to the quantum size effect. Zhao et al. [18] explored a redshift in the absorption spectrum of B-doped TiO$_2$ and explained the redshift as arising from crystal geometry modification of the electronic structures. In fact, B dopants can substitute for either O or Ti atoms, or can even sit in the interstitial sites. Density functional theory (DFT) calculations [19–21] suggest that B substitution for Ti atoms is energetically least favorable, while interstitial substitution and substitution for O are energetically comparable, so they can both occur in real situations. Patel et al. [21] suggested that at low concentration B preferentially occupies interstitial positions, but with increasing concentration B occupies lattice sites by replacing O.

Yang et al. [22] reported that P substitution for O narrows the band gap slightly by introducing impurity P 3p levels in the bandgap which could induce absorption edge redshift. Impurity level creation not only decreases the band gap but also provides centers promoting carrier recombination. Band gap reduction enhances visible light absorption but shortens carrier life by recombining carriers. The competition of these two effects determines the catalytic performance of TiO$_2$. However, P replacement of Ti produces no impurity energy levels though it narrows the band gap of the anatase TiO$_2$ slightly which is ineffective for photocatalytic improvement.

Recent progress indicates that codoping with B and P or with other nonmetals [8, 23–27] enhances UV-Vis light absorption when compared with monodoped TiO$_2$ due to "p-n pairs" [8] or the "synergistic effect" [25]. However, the effects of doping and codoping with B and P on the band structure of TiO$_2$ remain unclear. Here we systematically examine the effect of B- and P-doping and codoping on the electronic structures and optical properties of the anatase phase of TiO$_2$ using DFT calculations.

Materials and Methods

The present work was done using the spin-polarized DFT model of the CASTEP package [28]. The electron-ionic core interaction was represented using the ultra-soft pseudo-potential and the electron-electron interactions were described by the generalized gradient approximation (GGA) via the PW91 functional [29]. The structural optimizations were calculated using the plane-wave basis cutoff energy of 400 eV.

After structure optimization, we calculated the electronic structures and the optical properties of B- and P-doped and B/P-codoped TiO$_2$. However, traditional DFT usually cannot
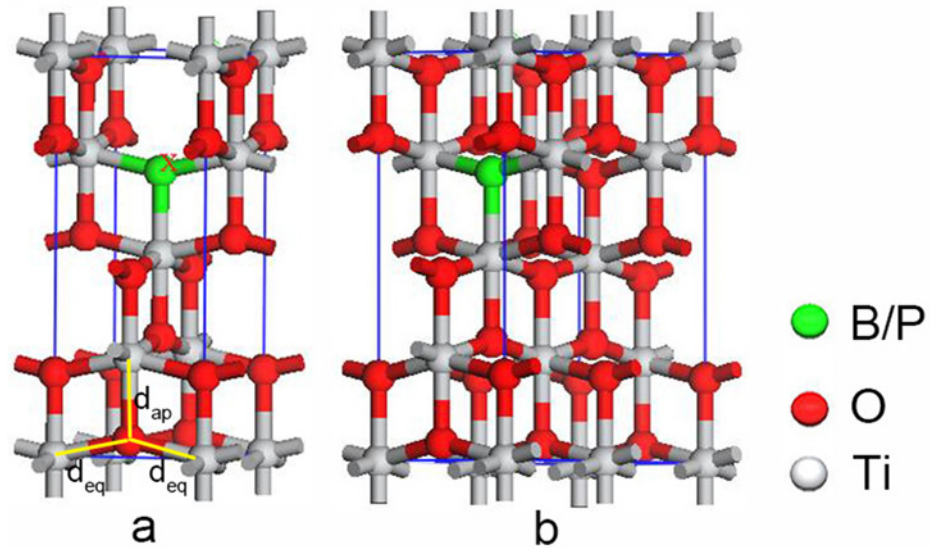
Fig 1. B(P) replacement of an oxygen atom in the (a) 1 × 1 × 1 and (b) 2 × 1 × 1 anatase TiO$_2$ supercells, the corresponding doping level is 8.3% and 4.2%, respectively. The d_{ap} and d_{eq} denote the apical and the equatorial bond lengths, respectively.

accurately describe the band gap of semiconductors. We considered that an on-site correction can get a band gap match more in line with experimental results as well as provide a more economical calculation than a hybrid functional correction, so the GGA+U method was an efficient way to study the electronic and optical properties [30–32]. It was shown that when $U = 4.25$ eV is applied to the Ti 3d electrons, the band gap of pure anatase TiO$_2$ is 3.20 eV, which corresponds well with experimental results. This U value has proven to be reasonable for dealing with impurity states in the bandgap [31] and in redox catalysis by TiO$_2$ [33].

Results and Discussion

B- or P-Doping

We replaced one O atom with a B or P atom in the 48-atom 2 × 2 × 1, 24-atom 2 × 1 × 1, and 12-atom 1 × 1 × 1 supercells of anatase TiO$_2$ shown in Fig 1 and denoted as (a) and (b) to simulate doping concentrations of 8.3% and 4.2%, respectively. Pure TiO$_2$ was used as a reference. The Monkhorst-Pack mesh was set as 5 × 5 × 4, 10 × 10 × 4, and 10 × 10 × 4 for these supercells. Optimized structural parameters of a, c, and d (d_{eq} and d_{ap} are the equatorial and apical Ti–O bond lengths, respectively) for the primitive unit cell of anatase TiO$_2$ (space group I4$_1$/amd) are shown in Table 1 which fits well with experimental observations [34] and HSE06 hybrid functional calculation results [35].

Table 1. Optimized structural parameters of the primitive unit cell of anatase TiO$_2$.

	Exp. [34]	HSE06 [35]	This work
a/Å	3.78	3.80	3.78
c/Å	9.50	9.47	9.49
d_{eq}/Å	1.93	1.94	1.95
d_{ap}/Å	1.98	1.98	2.00
c/a	2.51	2.49	2.51

Table 2. Formation energy, Mulliken populations on the B atom and the Ti(O) atoms bonded to the B atom, and bond lengths of the B–Ti(O) bonds for different B-doping concentrations.

Concentration (%)	Formation energy(eV)		Bond length (Å)			Mulliken population			Band gap (eV)
	Ti-rich	O-rich	Ti–O	B–Ti	B–O	Ti	O	B	
0	-	-	1.979/1.932(2)	-	-	1.48/1.34[22]	−0.74/−0.67[22]	-	3.2
2.1	7.09	10.69		-	1.371(2)	1.36(2)	−0.72(2)	0.27	2.84
4.2	10.89	14.49		2.352/2.074(2)		1.34(2) 1.41		−0.26	2.64
8.3	11.31	14.91		2.170/1.964(2)		1.21(2) 1.38		−0.37	0

doi:10.1371/journal.pone.0152726.t002

B-Doping

For comparison, the defect formation energy (E_{form}) can be calculated using the following formula

$$E_{\text{form}} = E_{\text{tot}}(\text{doped}) - [E_{\text{tot}}(\text{pure}) + \mu_x - \mu_O] \qquad (1)$$

where μ_x represents the chemical potential of x (x = B, P, O, and Ti) and $E_{\text{tot}}(\text{pure})$ and
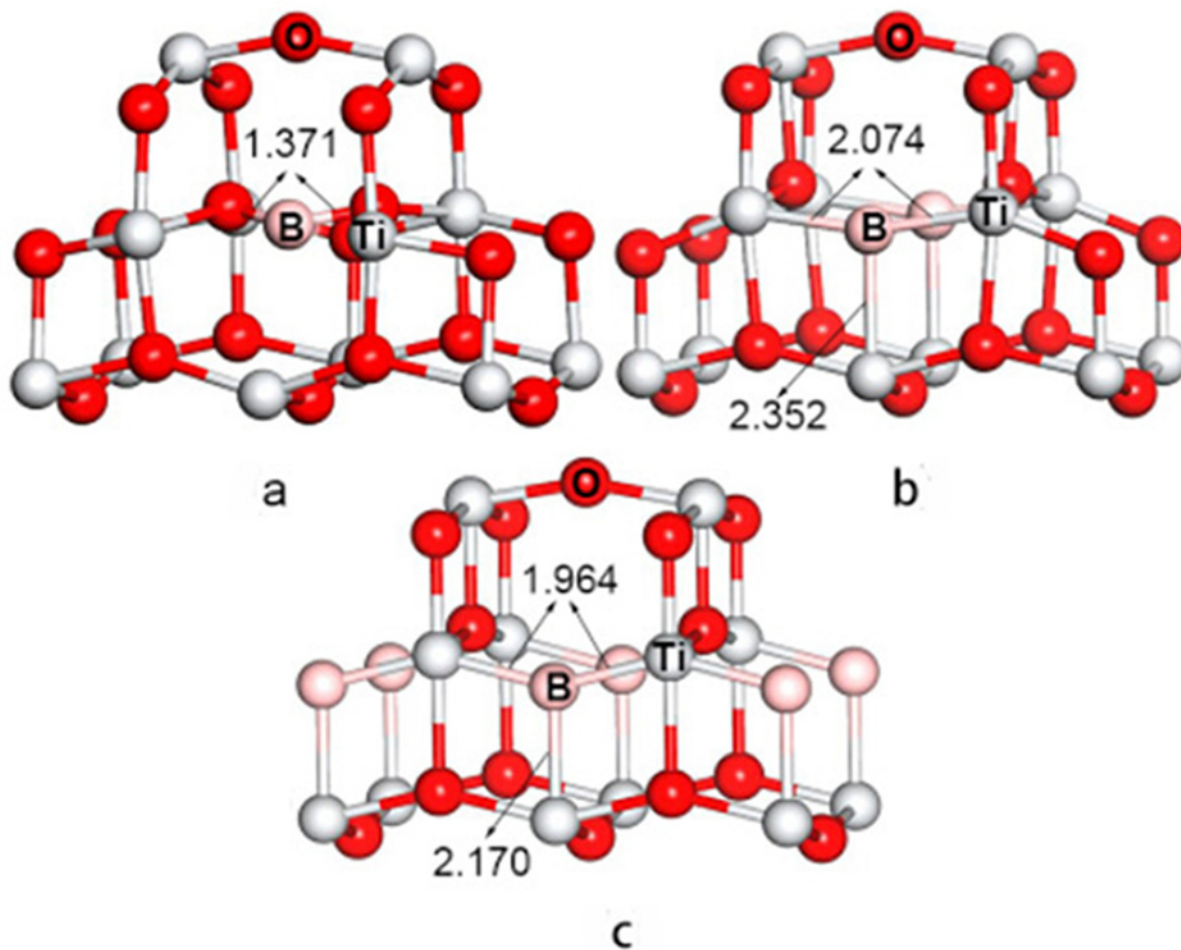
Fig 2. Partial geometries of the B-doped TiO$_2$ at (a) 2.1%, (b) 4.2%, (c) 8.3% doping concentrations.

doi:10.1371/journal.pone.0152726.g002
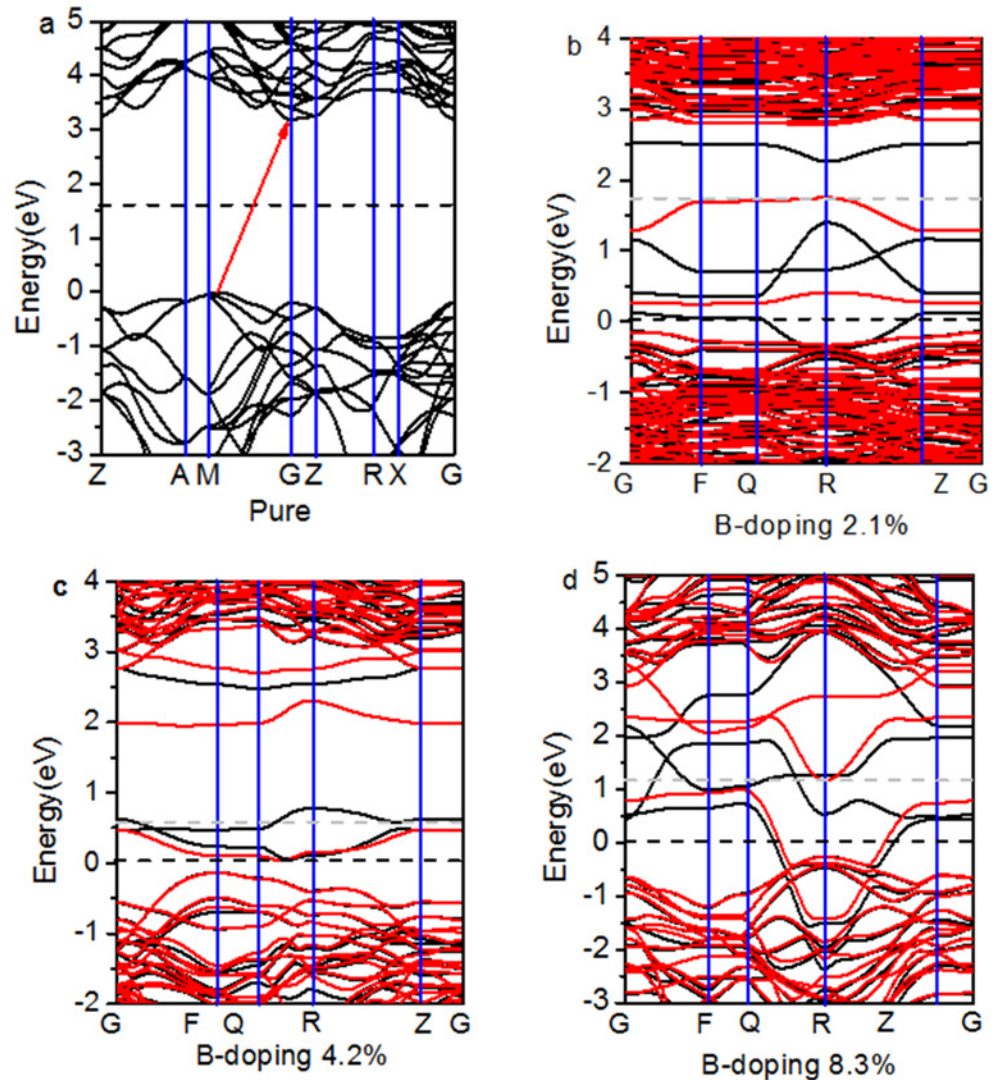
Fig 3. Band structures for (a) pure and B-doped TiO$_2$ at (b) 2.1%, (c) 4.2%, and (d) 8.3% doping concentrations. Black and red lines denote the spin up and down states, respectively. The energy is measured from the top of the valence band of pure anatase TiO$_2$.

E_{tot}(doped) are the total energies of pure and doped TiO$_2$, respectively. It is noteworthy that E_{form} is not fixed but that it changes with different growing conditions, such as Ti-rich, O-rich, or mixed conditions. The B chemical potential was given by the equation $\mu_B = 1/2E(B_2O_3)- 3/4E(O_2)$. Under Ti-rich conditions, the Ti chemical potential is assessed from the energy of bulk Ti while the O chemical potential was obtained from the following equation:

$$\mu_{Ti} + 2\mu_O = \mu(TiO_2) \tag{2}$$

Under O-rich conditions, the μ_O value is taken from the chemical potential of the free O$_2$ molecule, while the chemical potential of Ti is fixed by the conditions set by Eq 2. It is well known that the smaller the E_{form} value, the greater the stability of the doped TiO$_2$ supercell. The formation energies for various concentrations of B-doped TiO$_2$ are reported in Table 2. It is noted that for all concentrations of B doped into TiO$_2$, substitution of the lattice O is more
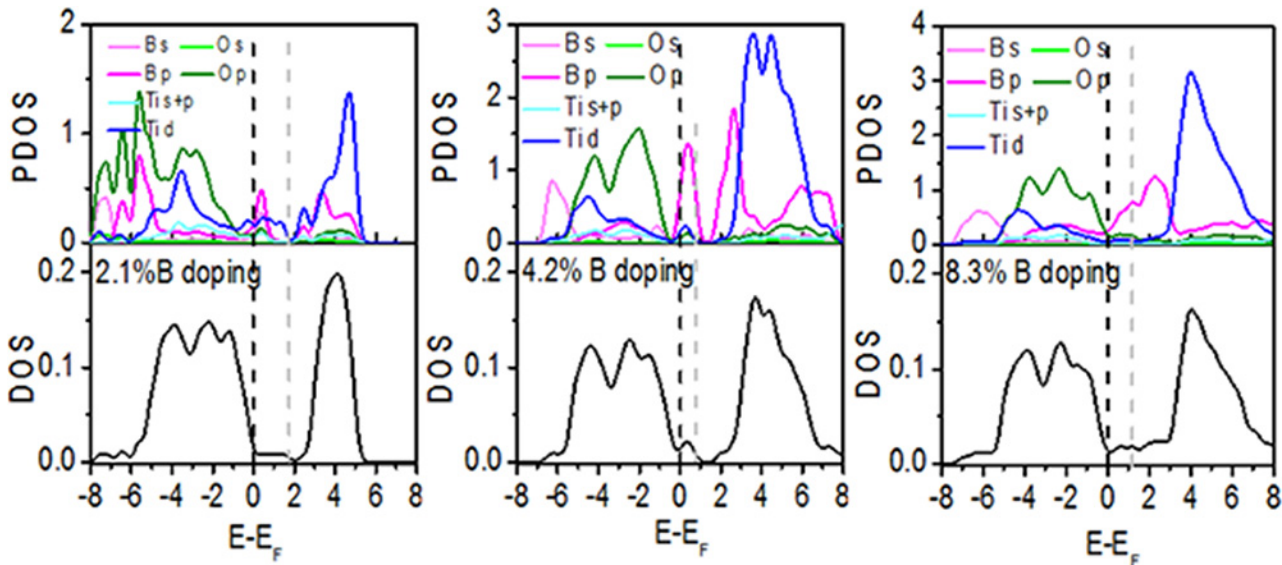
Fig 4. PDOS and normalized DOS for B-doped anatase TiO₂. The energy is measured from the top of the valence band of pure anatase TiO₂. The gray dotted line represents the actual Fermi level. PDOS is the average density of states of each atom near the defects.

doi:10.1371/journal.pone.0152726.g004

reasonable under the Ti-rich growth conditions and B-doping is increasingly difficult as the concentration increases.

The partial structures derived from the optimized B-doped TiO₂ with different doping concentrations are given in Fig 2. It is shown that high concentration (8.3% and 4.2%) doping does not distort the optimized crystal structure with elongation of the Ti–B bond. In the d_{eq} direction, the distances between B and Ti atoms stretch from the initial 1.932 Å to 1.964 and 2.074 Å, meanwhile, in the d_{ap} direction, the distances elongate from the initial 1.979 Å to 2.170 and 2.352 Å for 8.3% and 4.2% B-doping, respectively.

When the doping concentration is low (2.1%), the B atom deviates from its original position to instead bind with two neighboring O atoms to form a Ti–O–B bond in accordance with XPS measurements [21, 36]. Both B–O bonds are 1.371 Å. Furthermore, the Mulliken population study shows that the charges on the B atoms are about −0.37 and −0.26 for the 8.3% and 4.2% doping, respectively (see Table 2). The charge density is mainly distributed on the B atom rather than on the neighboring Ti and O atoms. At the 2.1% doping level, B atoms have a positive charge of 0.27 and form a Ti–O–B structure after the transfer of electrons from B to the adjacent O atoms.

The band structures of pure and B-doped anatase TiO₂ are shown in Fig 3. The conduction band minimum (CBM) and the valance band maximum (VBM) of pure TiO₂ appear on the gamma (G) and M points, respectively. The DFT+U calculations confirm an indirect band gap

Table 3. Formation energy, Mulliken populations on the P atom and the Ti atoms bonded to the P atom, and bond lengths of the P–Ti bonds for different doping concentrations.

Concentration (%)	Formation energy (eV)		Bond length (Å)		Mulliken population			Band gap (eV)
	Ti-rich	O-rich	Ti–O	P–Ti	Ti	O	P	
0	-	-	2.003/1.945(2)	-	1.48(1.34[22])	−0.74/(−0.67[22])	-	3.2
2.1	11.47	15.07		2.264/2.362/2.412	1.22/1.26/1.32		−0.17	3.12
4.2	12.86	16.46		2.235(2)/2.367	1.24(2)/1.36		−0.17	2.46
8.3	13.85	17.45		2.222(2)/2.318	1.09(2)/1.30		−0.26	0.75

doi:10.1371/journal.pone.0152726.t003
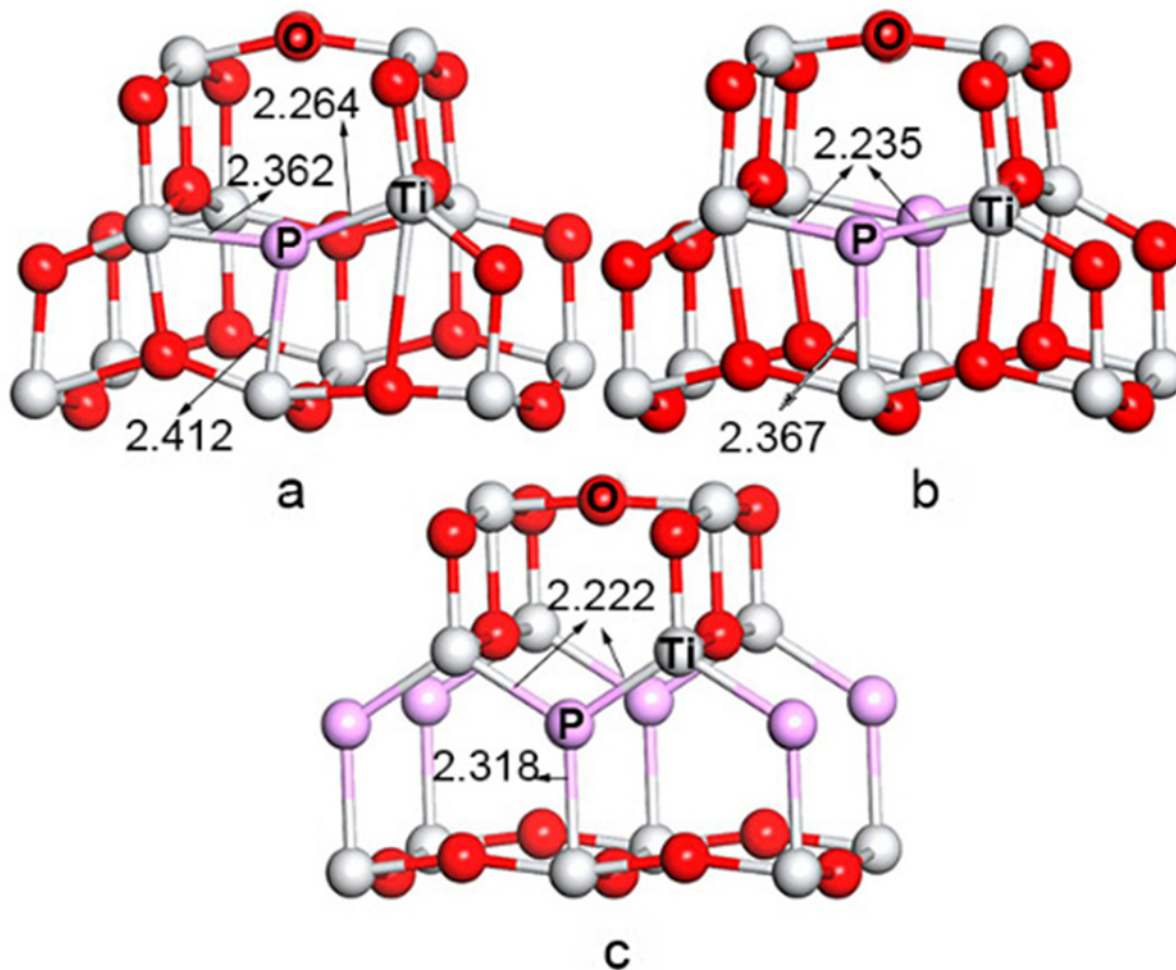
Fig 5. Partial geometries for P-doped TiO$_2$ at (a) 2.1%, (b) 4.2%, (c) 8.3% doping level.

of 3.20 eV for the anatase phase. Fig 3B–3D shows that the band gap decreases gradually with an increase in the doping concentration. The band gap approaches zero at the 8.3% doping level.

Fig 4 shows the projected density of states (PDOS) near the dopants and the total density of states (DOS) for B-doped TiO$_2$. The PDOS plots indicate that the O 2p states form most of the valence band while the conduction band is mainly composed of the Ti 3d states in B-doped TiO$_2$, which is consistent with pure TiO$_2$. B doped into TiO$_2$ does not produce a simple superposition of valence electrons but the process instead exchanges and polarizes electrons. First, some impurity energy levels emerge in the bandgap and they are mainly composed of B 2p electrons and neighboring Ti 3d and O 2p electrons. Second, the strong delocalization and bonding characteristics are formed by B 2s and O 2p electrons. Third, the valence and conduction bands gradually broaden with increased concentration of B-doping.

P-Doping

Substituting O sites with P in the TiO$_2$ was also examined for the same set of anatase TiO$_2$ supercells. The formation energies for P-doped anatase TiO$_2$ were also calculated according to Eqs (1) and (2), in which the chemical potential of phosphorus was obtained from the equation $\mu_P = 1/2E(P_2O_5) - 5/4E(O_2)$. Table 3 lists the optimal structural parameters. For all concentrations of P
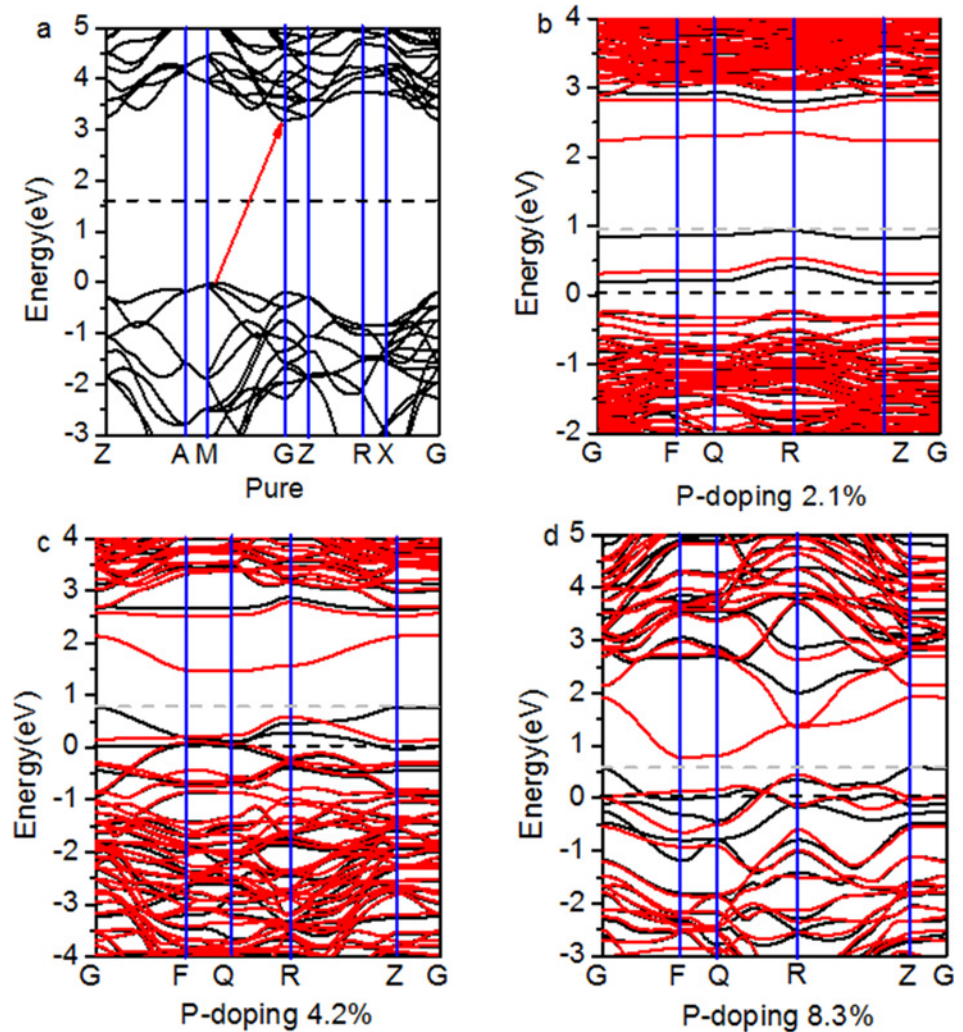
Fig 6. Band structures for (a) pure and P-doped TiO₂ at (b) 2.1%, (c) 4.2%, and (d) 8.3% doping levels. The energy is measured from the top of the valence band of pure anatase TiO₂.

doped into TiO₂, substitution of the lattice O is reasonable under the Ti-rich growth conditions and P-doping becomes increasingly difficult as the concentration increases.

Fig 5 shows the local geometries taken from different P-doping concentrations in the anatase TiO₂ supercells. This case is similar to B-doping because the distances between the P atom and adjacent Ti atoms shorten with increasing concentration, while an asymmetric structure deformation occurred for 2.1% P-doping (d_{eq} = 2.222 Å, d_{ap} = 2.318 Å for 8.3% doping level; d_{eq} = 2.235 Å, d_{ap} = 2.367 Å for 4.2% doping level; d_{eq} = 2.264 Å and 2.362 Å, d_{ap} = 2.412 Å for 2.1% doping level). These differences for both the B- and P-doped structures are larger than the original Ti–O bond length due to the larger B and P atomic radii. Moreover, considering the lower electronegativity of P than B and O, the charge on P in P-doped anatase TiO₂ is more mobile than on B and O due to weaker ionic interactions between the P anion and adjacent Ti cation, and thus fewer electrons are transferred from Ti to P (see Table 3).

Fig 6 shows that P-doping reduces the band gap to 3.12 eV for the 2.1% doping level, 2.46 eV for the 4.2% doping level, and 0.75 eV for the 8.3% doping concentrations. Fig 7 shows the PDOS and DOS due to different concentrations of dopant. Characteristics of the B-doped TiO₂ DOS
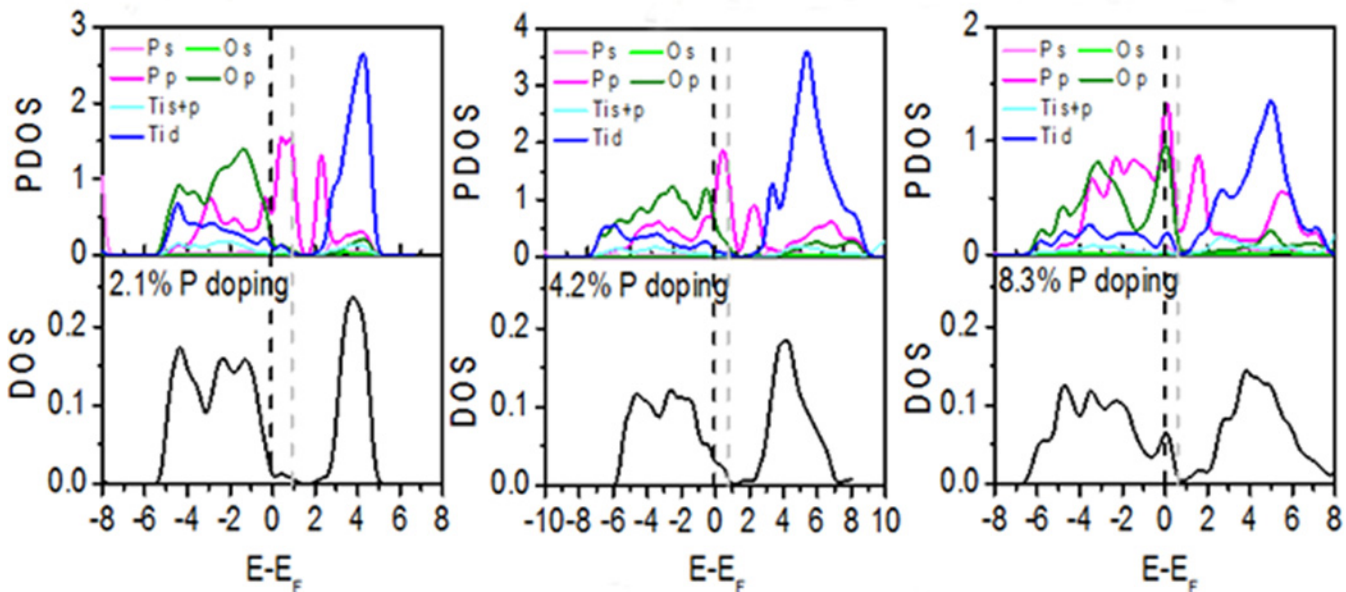
Fig 7. PDOS and normalized DOS for P-doped anatase TiO$_2$. The energy is measured from the top of the valence band of pure anatase TiO$_2$. The gray dotted line represents the actual Fermi level. PDOS is the average density of states of each atom near the defects.

also similarly appear in the P-doped TiO$_2$. P doped into TiO$_2$ also exchanges and polarizes valence electrons of pure TiO$_2$. First, some impurity energy levels emerge in the bandgap that are mainly composed of the P 3p electrons and neighboring Ti 3d and O 2p electrons. Second, the strong delocalization and bonding characteristics are formed by P 3p and O 2p electrons. Third, the valence and conduction bands gradually broaden with increased concentration of P-doping.

In Fig 8, zone-selective photoelectron spectroscopy (ZPS) technology [37] is used to determine the changes in the electronic structure for different concentrations of B and P doped into TiO$_2$. The results clarified that additional DOS features are formed in all B- and P-doped TiO$_2$. Entrapped states within the band gap as impurity states enhance the utilization of visible light
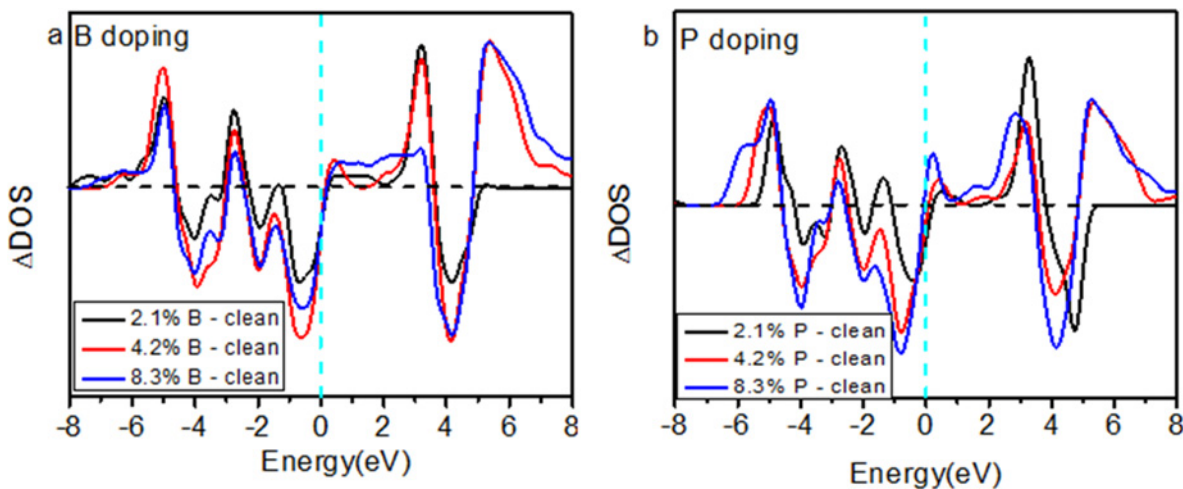
Fig 8. The residual DOS for B- (a) and P- (b) doped TiO$_2$ at 2.1%, 4.2%, and 8.3% doping concentrations.
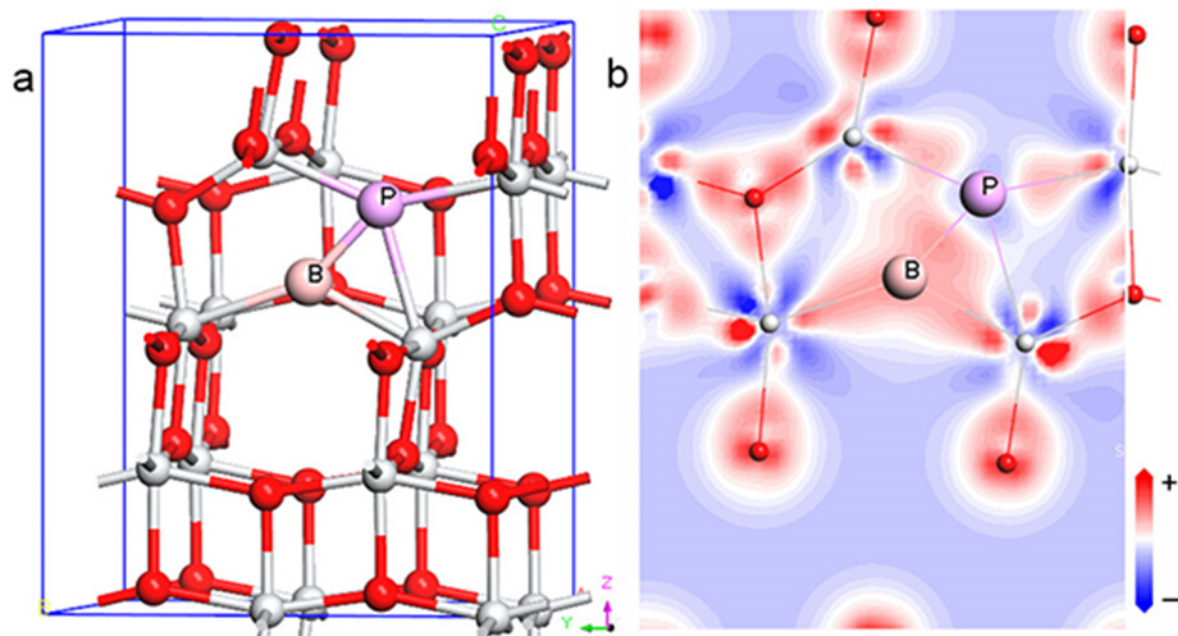
Fig 9. (a) Optimized geometries for the B- and P-codoped TiO$_2$, and (b) corresponding difference electron density maps for the plane with B and P atoms.
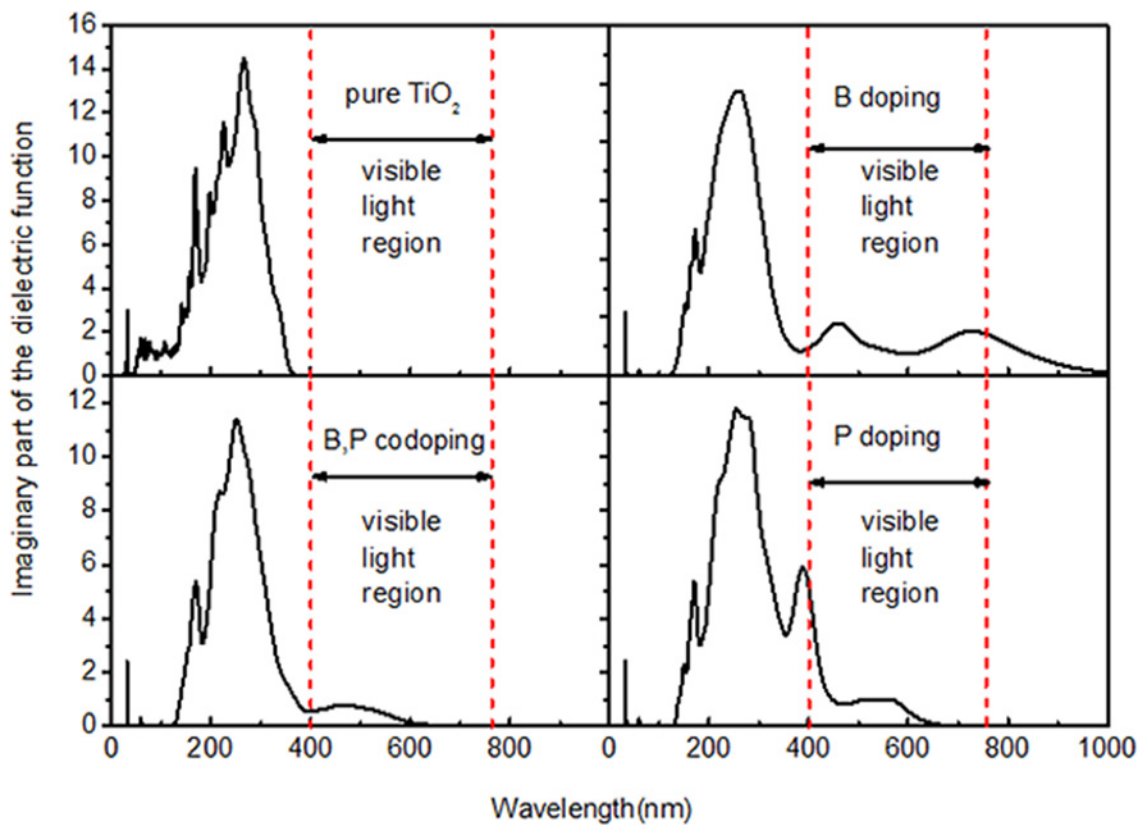
Fig 10. Calculated imaginary part of the dielectric function (ε_2) for pure, monodoped, and codoped TiO$_2$. The region between the horizontal dashed lines marks the visible light region.
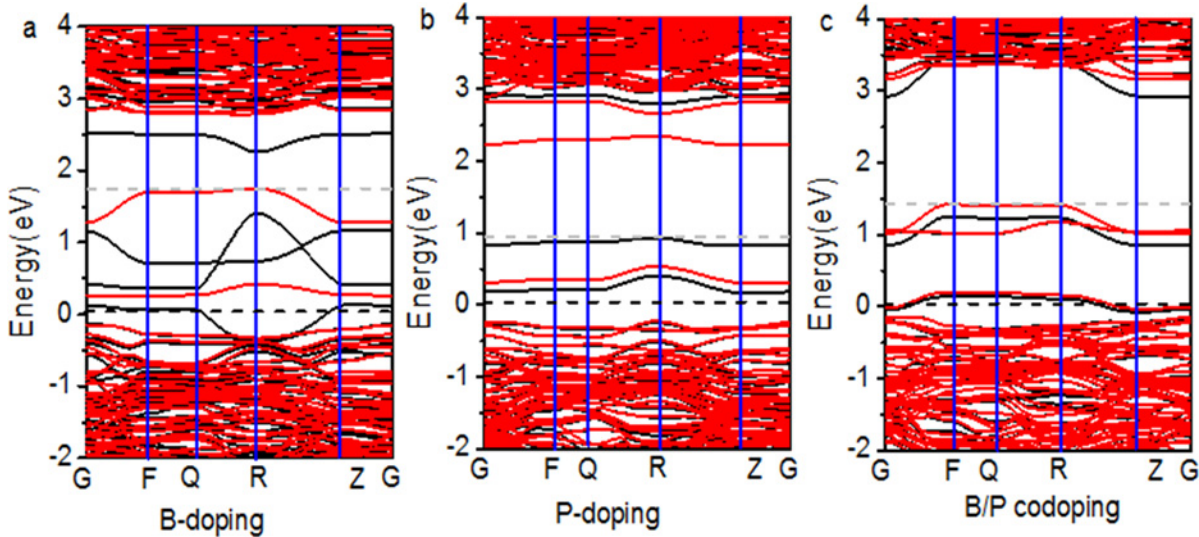
Fig 11. Band structures of (a) B-, (b) P-, and (c) B/P-codoped. The energy is measured from the top of the valence band of pure anatase TiO$_2$. The gray dotted line represents the actual Fermi level.

and the antibonding states polarize the Ti 3d electrons by entrapped states, thus decreasing the work function contributing to catalytic ability, which have been proven in previous reports [38].

B- and P-Codoping

To investigate the stabilities of B- and P-codoped systems, we studied the E_{form} for two O atoms: one replaced by a B atom and one replaced by a P atom in the 48-atom ($2 \times 2 \times 1$) supercell. Note that the increasing distance between the B and P atoms in both Ti-rich and O-rich growing conditions leads to an increase in E_{form}. B and P atoms substituting the nearest neighboring O atoms are energetically more favorable. Fig 9 shows the optimized structure and the electron density distribution. The B and P atoms form a new B–P bond of length d = 1.775 Å. This bond is shorter than the sum of the atomic radii: 0.95 (B) + 1.30 (P) = 2.25 Å, which means a stronger B–P single bond is formed as compared to the original O–O separation in pure TiO$_2$ of 2.474 Å. The difference charge map also shows that B gains electron from P.

To further validate the influence of doping on light absorption, we compared the imaginary part of the dielectric function (ε_2), which is an important parameter for photoresponse testing (Fig 10). The calculated ε_2 for pure TiO$_2$ is in agreement with a recent experiment [39]. It is obvious that all B-, P-, and B/P-codoped TiO$_2$ can achieve absorption of visible light and the absorption edges decrease relatively from pure TiO$_2$ by 1.89, 1.32, and 1.15 eV, respectively.

The band structures of B-doped, P-doped, and B/P-codoped are compared in Fig 11. Because of the synergistic effect of B and P, unoccupied energy levels at the bottom of the CBM are quenched which act as a recombination center in B-doped and P-doped TiO$_2$. Moreover, it is worth noting that the CBM and the VBM determine the reducing and oxidizing ability. As the VBM gets lower compared with the hydrogen production level, the oxidizing ability increases. Similarly, as the CBM gets higher, the reducing ability increases. Since the CBM of pure TiO$_2$ is slightly higher than the hydrogen production level, it is best to either keep the position of the CBM unchanged or raise it in the process of band structure modulation. Because B and P passivated codoping can decrease the band gap, as well as avoid changes to the CBM compared with the B-doped and P-doped TiO$_2$, codoping produces a suitable visible-light absorption region and doesn't handicap the reducing power of TiO$_2$.

Conclusions

In summary, we investigated the effects of B-doping, P-doping, and B/P-codoping on the electronic structures and optical properties of anatase TiO$_2$ by employing DFT calculations. Non-metal doping, such as that with B and P, does not produce a simple superposition of valence electrons, but instead the process exchanges and polarizes electrons compared to pure TiO$_2$. Localized entrapped states in the band gap can absorb visible light and the polarization states induced by entrapped states decrease the work function to improve the reactivity of the carriers. Moreover, B and P passivated codoping quenches the unoccupied energy levels to prolong the carrier lifetime and cause less perturbation to the CBM, thus resulting in a suitable visible-light absorption region that does not handicap the reducing power of TiO$_2$.

Acknowledgments

Author Contributions

Conceived and designed the experiments: LL FLM HWT WTZ CQS. Performed the experiments: LL LQ XYH. Analyzed the data: LL HWT LQ XYH WTZ CQS. Wrote the paper: LL CQS.

References

1. Sun CQ. Relaxation of the Chemical Bond. Heidelberg New York Dordrecht London Singapore 2014 Berlin: Springer press; ISBN:978-981-4585-20-0. 550 p.

2. Li L, Tian H-W, Meng F-L, Hu X-Y, Zheng W-T, Sun CQ. Defects improved photocatalytic ability of TiO2. Appl Surf Sci. 2014; 317:568–72.

3. Wendt S, Sprunger PT, Lira E, Madsen GK, Li Z, Hansen JO, et al. The role of interstitial sites in the Ti3d defect state in the band gap of titania. Science. 2008; 320(5884):1755–9. doi: 10.1126/science.1159846 PMID: 18535207

4. Asahi R, Morikawa T, Ohwaki T, Aoki K, Taga Y. Visible-light photocatalysis in nitrogen-doped titanium oxides. Science. 2001; 293(5528):269–71. PMID: 11452117

5. Li C, Zhao YF, Gong Y, Wang T, Sun CQ. Band gap engineering of early transition-metal-doped anatase TiO2: first principles calculations. Phys Chem Chem Phys. 2014; 16:21446–51. doi: 10.1039/c4cp03587a PMID: 25183457

6. Grabowska E, Zaleska A, Sobczak JW, Gazda M, Hupka J. Boron-doped TiO2: Characteristics and photoactivity under visible light. Procedia Chemistry. 2009; 1(2):1553–9.

7. Giannakas AE, Seristatidou E, Deligiannakis Y, Konstantinou I. Photocatalytic activity of N-doped and N–F co-doped TiO2 and reduction of chromium(VI) in aqueous solution: An EPR study. Appl Catal, B. 2013; 132–133:460–8.

8. Wang P, Liu Z, Lin F, Zhou G, Wu J, Duan W, et al. Optimizing photoelectrochemical properties of TiO_{2} by chemical codoping. Phys Rev B. 2010; 82(19):193103.

9. Gai Y, Li J, Li S-S, Xia J-B, Wei S-H. Design of Narrow-Gap TiO2: A Passivated Codoping Approach for Enhanced Photoelectrochemical Activity. Phys Rev Lett. 2009; 102:036402. PMID: 19257373

10. Yu D, Zhou W, Liu Y, Zhou B, Wu P. Density functional theory study of the structural, electronic and optical properties of C-doped anatase TiO2 (101) surface. Phys Lett A. 2015; 379(28–29):1666–70.

11. Huang J, Buyukcakir O, Mara MW, Coskun A, Dimitrijevic NM, Barin G, et al. Highly efficient ultrafast electron injection from the singlet MLCT excited state of copper(I) diimine complexes to TiO2 nanoparticles. Angew Chem Int Ed. 2012; 51(51):12711–5.

12. Andrei C, Lestini E, Crosbie S, de Frein C, O'Reilly T, Zerulla D. Plasmonic enhancement of dye sensitized solar cells via a tailored size-distribution of chemically functionalized gold nanoparticles. PLoS One. 2014; 9(10):e109836. doi: 10.1371/journal.pone.0109836 PMID: 25354362

13. Weiher N, Beesley AM, Tsapatsaris N, Delannoy L, Louis C, Bokhoven JAv, et al. Activation of oxygen by metallic gold in Au/TiO2 catalysts. J Am Chem Soc. 2007.

14. Hou Q, Zhao C, Guo S, Mao F, Zhang Y. Effect on Electron Structure and Magneto-Optic Property of Heavy W-Doped Anatase TiO2. PLoS One. 2015; 10(5):e0122620. doi: 10.1371/journal.pone.0122620 PMID: 25955308

15. Schrauben JN, Hayoun R, Valdez CN, Braten M, Fridley L, Mayer JM. Titanium and zinc oxide nano-particles are proton-coupled electron transfer agents. Science. 2012; 336:1298–301. doi: 10.1126/science.1220234 PMID: 22679095

16. Bansal V, Yang D, Fan T, Zhou H, Ding J, Zhang D. Biogenic Hierarchical TiO2/SiO2 Derived from Rice Husk and Enhanced Photocatalytic Properties for Dye Degradation. PLoS ONE. 2011; 6(9): e24788. doi: 10.1371/journal.pone.0024788 PMID: 21931853

17. Chen D, Yang D, Wang Q, Jiang Z. Effects of Boron Doping on Photocatalytic Activity and Microstructure of Titanium Dioxide Nanoparticles. Ind Eng Chem Res. 2006; 45:4110–6.

18. Zhao W, Ma W, Chen C, Zhao J, Shuai Z. Efficient Degradation of Toxic Organic Pollutants with Ni₂O₃/TiO₂₋ₓBₓ under Visible Irradiation. J Am Chem Soc. 2004; 126:4782–3. PMID: 15080674

19. Geng H, Yin S, Yang X, Shuai Z, Liu B. Geometric and electronic structures of the boron-doped photo-catalyst TiO2. J Phys Condens Matter. 2006; 18(1):87–96.

20. Fittipaldi M, Gombac V, Montini T, Fornasiero P, Graziani M. A high-frequency (95GHz) electron para-magnetic resonance study of B-doped TiO2 photocatalysts. Inorg Chim Acta. 2008; 361(14–15):3980–7.

21. Patel N, Dashora A, Jaiswal R, Fernandes R, Yadav M, Kothari DC, et al. Experimental and Theoretical Investigations on the Activity and Stability of Substitutional and Interstitial Boron in TiO2Photocatalyst. J Chem Phys. 2015; 119(32):18581–90.

22. Yang K, Dai Y, Huang B. Understanding Photocatalytic Activity of S- and P-Doped TiO₂ under Visible Light from First-Principles. J Phys Chem C. 2007; 111:18985–94.

23. Feng N, Zheng A, Wang Q, Ren P, Gao X, Liu S- B, et al. Boron Environments in B-Doped and (B, N)-Codoped TiO2Photocatalysts: A Combined Solid-State NMR and Theoretical Calculation Study. J Phys Chem C. 2011; 115(6):2709–19.

24. Wu Y, Xing M, Zhang J, Chen F. Effective visible light-active boron and carbon modified TiO2 photocatalyst for degradation of organic pollutant. Appl Catal, B. 2010; 97(1–2):182–9.

25. Lin Y, Jiang Z, Zhu C, Hu X, Zhang X, Zhu H, et al. C/B codoping effect on band gap narrowing and optical performance of TiO2 photocatalyst: a spin-polarized DFT study. J Mater Chem A. 2013; 1(14):4516.

26. Lin L, Zheng RY, Xie JL, Zhu YX, Xie YC. Synthesis and characterization of phosphor and nitrogen co-doped titania. Appl Catal, B. 2007; 76(1–2):196–202.

27. Liu G, Zhao Y, Sun C, Li F, Lu GQ, Cheng HM. Synergistic effects of B/N doping on the visible-light photocatalytic activity of mesoporous TiO2. Angew Chem Int Ed. 2008; 47(24):4516–20.

28. Segall M, Lindan PJD, Probert MJ, Pickard CJ, Hasnip PJ, Clark SJ, et al. First-principles simulation: ideas, illustrations and the CASTEP code. J Phys: Condens Matter 2002; 14 2717–44.

29. Perdew J, Ziesche P, Eschrig H. Chapter Unified Theory of Exchange and Correlation Beyond the Local Density Approximation1991.

30. Allen JP, Watson GW. Occupation matrix control of d- and f-electron localisations using DFT + U. Phys Chem Chem Phys. 2014; 16:21016. doi: 10.1039/c4cp01083c PMID: 24832683

31. Finazzi E, Di Valentin C, Pacchioni G, Selloni A. Excess electron states in reduced bulk anatase TiO₂: comparison of standard GGA, GGA+U, and hybrid DFT calculations. J Chem Phys. 2008; 129 (15):154113. doi: 10.1063/1.2996362 PMID: 19045182

32. Zhu HX, Zhou PX, Li X, Liu JM. Electronic structures and optical properties of rutile TiO2 with different point defects from DFT+U calculations. Phys Lett A. 2014; 378(36):2719–24.

33. Hu Z, Metiu H. Choice ofUfor DFT+UCalculations for Titanium Oxides. J Phys Chem C. 2011; 115 (13):5841–5.

34. Burdett JK, Hughbanks T, Miller GJ, Richardson JW, Smith JV. Structural-Electronic Relationships in Inorganic Solids: Powder Neutron Diffraction Studies of the Rutile and Anatase Polymorphs of Titanium Dioxide at 15 and 295 K. J Am Chem Soc. 1987; 109:3639–46.

35. Liu Y, Zhou W, Liang Y, Cui W, Wu P. Tailoring Band Structure of TiO2to Enhance Photoelectrochemical Activity by Codoping S and Mg. J Phys Chem C. 2015:150505122422009.

36. Zaleska A, Grabowska E, Sobczak JW, Gazda M, Hupka J. Photocatalytic activity of boron-modified TiO2 under visible light: The effect of boron content, calcination temperature and TiO2 matrix. Appl Catal, B. 2009; 89(3–4):469–75.

37. Sun CQ, inventorAtomic scale purification of electron spectroscopic information (USA patent: publication: US20130090865). USA18, June 2010 17 December 2012.

38. Li L, Meng F, Tian H, Hu X, Zheng W, Sun CQ. Oxygenation mediating the valence density-of-states and work function of Ti(0001) skin. Phys Chem Chem Phys. 2015; 17(15):9867–72. doi: 10.1039/c4cp05985a PMID: 25777318

39. Asahi R, Taga Y. Electronic and optical properties of anatase TiO$_2$. Phys Rev B. 2000; 61:7459–65.